HBS: a Handheld Breast Cancer Detector Based on Frequency Domain Photon Migration with Full Heterodyne

Keun Sik No, Qiang Xie, Richard Kwong*, Albert Cerussi*, Bruce J. Tromberg*, Pai H. Chou
University of California, Irvine, CA 92697-2625 USA, *Beckman Laser Institute and Medical Clinic, University of California, Irvine, CA

***Abstract*— HBS, for Handheld Breast Scanner, is a miniature medical instrument for non-invasive breast cancer detection based on the principle of frequency domain photon migration spectroscopy. It performs content-based analysis by deriving scattering and absorption coefficients from amplitude and phase differences in backscattered, broadband-modulated (10MHz to 1GHz) near-infrared light. This paper reports improvements made in the latest HBS design over the previous design, called the Mini-FDPM. First, it uses full heterodyne detection to significantly improve the sensitivity, so that fiber coupling can be used instead of being limited to direct laser contact only. Second, the new firmware called Tapper accelerates the control speed while enabling HBSs to form a network. Experimental results show that HBS to have similar accuracy to the reference design, Laser Breast Scanner (LBS) currently in clinical trials.**

I. Introduction

Much progress has been recently made in improving breast cancer detection sensitivity specifically. Among many techniques developed to date, Near-Infrared Spectroscopy, specifically Frequency Domain Photon Migration (FDPM), is a *content-based* rather than an *image-based* method. It derives absorption (μ_a) and reduced scattering (μ_s') coefficients of tissue based on backscattered light in the near-infrared (NIR) light (600nm $\leq \lambda \leq$ 1300nm) regime. The NIR is modulated by RF frequency from 10MHz to 1GHz and an instrument measures the phase shift and attenuation (amplitude) of the backscattered light. Diffusion theory based modeling techniques use this acquired data to distinguish scattering from absorption events. This enables analysis of tissue physiological composition in terms of water, lipid, hemoglobin, and deoxyhemoglobin, along with tissue architecture (cellular and matrix) which have been shown to enable tumor detection in ways that complement image-based techniques [1].

A. Mini-FDPM

FDPM based technologies can be miniaturized and dramatically reduced in cost. The components and system architecture of an FDPM instrument are similar to those used in broadband RF and optical communication. In a prior publication, we have shown such a board-level prototype instrument named the Mini-FDPM [2]. It is a handheld unit that performs broadband modulation to drive one laser, and it performs homodyne phase detection and either heterodyne or homodyne amplitude detection. The Mini-FDPM assumes direct laser contact with the tissue, which was shown to be sufficiently accurate compared to the much larger reference prototype named Laser Breast Scanner (LBS).

However, this design has several limitations. First, despite recent progress in silicon lasers, it is still not easy for one laser diode to generate the 600nm to 1300nm spectrum with sufficient power output, while other devices are too bulky. Second, while direct contact of the laser on tissue is power efficient, fiber coupling is often still required to work with existing infrastructures. However, the coupling loss and longer detection path in this case translate into higher detection error. Therefore, methods for higher sensitivity is needed.

B. New Design: HBS

To address these problems, we designed and implemented a new system named H^2B^2S, for full-Heterodyne Handheld Broadband Breast Scanner, or simply HBS. To cover the NIR spectrum, we implement four laser drivers for four laser wavelengths. To increase sensitivity, we analyze the previous design for potential sources of noise and implement a new full-heterodyne design on both phase and amplitude detection paths. The third improvement is an order of magnitude acceleration in digital control, thereby enabling much faster detection and possibly real-time imaging. Experimental results on phantom tissues show that the HBS to have similar accuracy as the LBS with identical assumptions. It will be ready to serve as not only an LBS replacement but also a platform for a new generation of networked instruments.

II. Full Heterodyne RF Circuitry

The original FDPM concept is to generate an RF signal to amplitude modulate the laser light, and the receiver converts the light back to an RF signal for measuring the amplitude and phase shift relative to the original signal. The first Mini-FDPM design used homodyne detection, but its results deviated from the predictions of the diffusion theory and those of the reference design. The problem was that the laser light acted as a carrier for the RF signal, which suffered from much noise in the ambient light and harmonic frequency on the optical detection path.

To solve this problem, the second Mini-FDPM design used heterodyne detection for amplitude. Heterodyning is a classical tuning technique, where the carrier signal at frequency f is mixed with another signal at frequency $f+\Delta$ to generate a new lower-frequency carrier at $|\Delta|$. Originally designed to facilitate demodulation using lower frequency technologies, heterodyning in this case improves the sensitivity of signal detection by helping the Mini-FDPM filter out most of the noise due to ambient light and harmonics. We also added a sharp crystal filter to this heterodyne structure to further suppress noise, such that the resulting amplitude value follows the diffusion theory very well.

The results above were collected by direct laser contact to phantoms. Direct laser contact represents the ideal architecture, because it minimizes signal path and maximizes detection signal strength. This detected modulated laser light has high intensity and therefore a high RF signal-to-noise ratio. However, this setup has limited the use to one laser, even though it is important to sweep the optical spectrum to more clearly cover each of the four cancer identifiers at their peak optical frequencies. Currently, laser diodes are limited to a single wavelength each. Optical fiber coupling of multiple laser diodes can

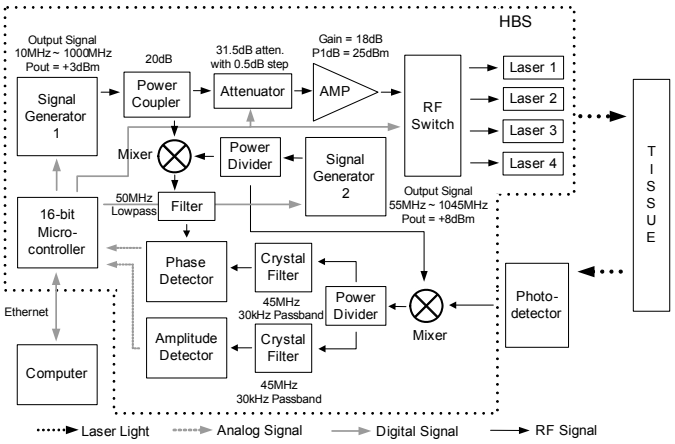

Fig. 1. Schematic of HBS

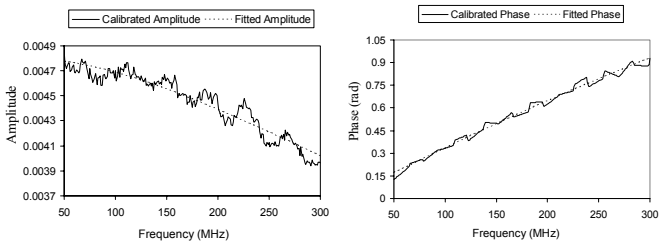

(a) (b)

Fig. 2. Results from amplitude-heterodyne Mini-FDPM: calibrated and fitted (a) Amplitude (b) Phase of Breast phantom

solve this problem, but there is more phase variation due to the longer detection path and a loss due to the fiber coupling. Unfortunately, results collected on the Mini-FDPM with fiber coupling show much higher noise in the detected phase, even though the amplitude matches well. Unlike the noise in the amplitude, the phase error is more sensitive to the signal path. If the signal travels a longer path, then it experiences a larger phase delay, and therefore it induces more phase error with same phase detection accuracy. In order to increase the accuracy, we applied heterodyning to phase detection on the version of Mini-FDPM that already performs heterodyne amplitude detection.

Fig. 1 shows the schematic of the full heterodyne structure. For every frequency f generated by the main signal generator, the second signal generator generates $f + 45$MHz to downconvert the demodulated RF signal as well as coupled modulated signal. This constant 45MHz signal is filtered by a crystal filter with 30KHz bandwidth to eliminate unwanted signals and reduce the noise floor. The differences between amplitude-only heterodyne and full heterodyne (i.e., both amplitude and phase) are shown in Figs. 2 and 3. Fig. 2 shows the measured and calibrated amplitude and phase results of the Breast phantom as measured by the (amplitude-only heterodyne) Mini-FDPM. We use Top1 phantom as reference amplitude for calibration, and the source-detector separation is 15mm. Fig. 3 shows the results from the HBS. It is clear that the amplitude and phase results from the HBS match much more closely with those predicted by the diffusion theory, due to the greatly reduced noise.

III. Laser Drivers

Because the tissue consists of multiple materials with different optical properties, it is important to take measurements for different

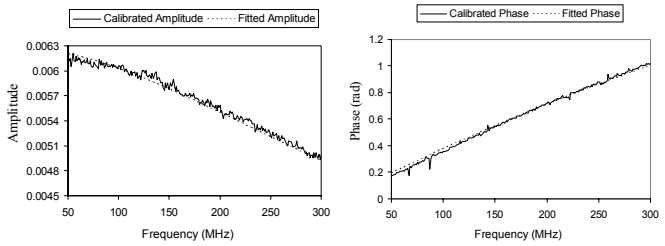

(a) (b)

Fig. 3. Results from HBS: calibrated and fitted (a) Amplitude (b) Phase of Breast phantom

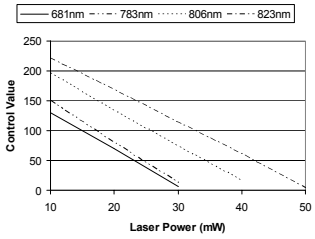

Fig. 4. Laser power with digital potentiometer value

optical wavelengths in order to determine their concentrations more precisely. Our new HBS has improved sensitivity such that it can still perform detection accurately even after a laser diode is coupled to a fiber before emitting into the tissue. Fiber coupling also enables the fibers connected to different laser diodes to be bundled in one spot small enough to be considered the same position. This way, the HBS can turn on one laser at a time for amplitude modulation from 10MHz–1GHz.

The primary question is how many wavelengths are needed. The current reference instrument, LBS, is using 6 discrete wavelength lasers diodes. Theoretically, only 4 lasers are needed to recover the optical properties of 4 unknown major absorbers of tissue. Although the more laser helps to increase the accuracy, HBS uses 4 lasers at 681nm, 783nm, 806nm, and 823nm which are sufficient to recover the necessary chromophore concentrations.

To power these lasers, HBS has four laser drivers, which are APC (automatic power control) circuits. Two APC circuits are for CAC (common laser diode anode and photodiode cathode) lasers and the others are for CCA (common laser diode cathode and photodiode anode) lasers. The power of each laser is controlled by a digital potentiometer with 256 steps. Fig. 4 shows the power of four lasers by digital potentiometer control values.

IV. Software Architecture

HBS adopts Tapper [3] as its new software archicture, and Rappit [4] as its user interface. Tapper features a scripting engine built on top of a set of low level application programming interfaces (APIs). The lightweight scripting engine parses user scripts and invokes system services supported by the underlying HBS hardware platforms. Rappit is the host-side software that used in conjunction with Tapper for *host-assisted* execution.

A. Host-Assisted Scripting Environment

To make HBS run as efficiently as possible with maximum flexibility and interactivity, we take the approach of host-assisted scripting. It means that the host software (Rappit) not only provides

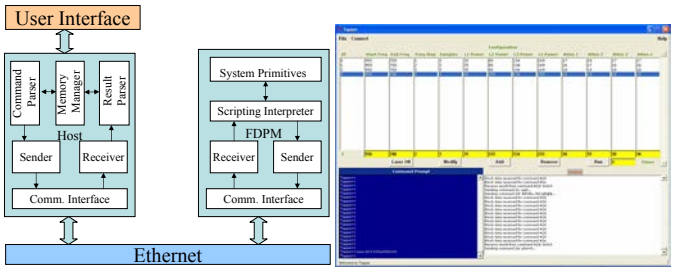

(a) (b)

Fig. 5. (a) Rappit/Tapper software architecture (b) Screenshot

a graphical user interface (GUI) but also pre-processes commands issued by the user before sending them over to the HBS. HBS itself runs the Tapper to interpret commands in the form of a script. The entire environment is shown in Fig. 5(a).

Rappit provides a command line interface (CLI) for the user to type in commands to HBS interactively. A GUI can also generate the commands and reformat results graphically. Input from the user can be classfied into host commands and target commands. Host commands are those executed on the host computer, e.g. saving data to a file, whereas target commands are those that are actually sent to the target HBS, e.g. setting GPIO value, start sweeping, set the amplifier power, etc. The parser parses the data, displays the results in the GUI, and stores them in a table, tagged by their ID. The host also runs the memory manager that keeps track of the data and flash memory usage at runtime and helps allocate/deallocate memory space on HBS.

Fig. 5(b) shows the GUI for the HBS application. The top window shows a list of HBS parameters the users can configure, including the start and end frequencies, the size of a frequency step, the number of samples, the laser power level, and the attenuation level. The CLI in the bottom-left corner provides full low-level access to the HBS for interactive hardware debugging. For example, they can turn on a laser by typing the command "ph6=1". The output is displayed in the bottom-right window.

V. Measurement Results

The measurement setup is shown in Fig. 6(a). The four laser diodes (681, 783, 806, and 823nm) are run sequentially at 20mW optical power. An optical fiber bundle with four 400μm diameter fibers is coupled to the four laser sources. The Hamamatsu C5658 avalanche photodiode detector and the optical fiber bundle are attached 15mm apart on the tissue-simulating phantoms with known optical properties. Each laser is modulated from 50MHz to 300MHz in 1MHz steps with the maximum available power without saturating the modulation at the 50MHz frequency. Although the HBS was designed for up to 1GHz, the reason we measured up to a 300MHz frequency range is due to the significant signal losses at higher frequencies in higher absorption phantoms such as the Muscle phantom.

A. Extracted Optical Properties

We measured a total of three phantoms, where one phantom was used as the calibration reference and the other two, Breast and Muscle, were sample phantoms. The Breast phantom was designed with both a lower overall absorption and higher reduced scattering coefficients similar to typical normal breast tissue. On the other hand, the Muscle phantom was designed with both higher overall absorption and lower reduced scattering coefficients similar to muscle tissues. The true optical properties of each phantom were characterized

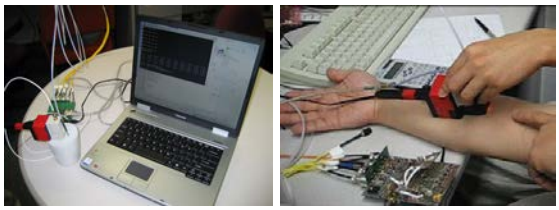

(a) (b)

Fig. 6. (a) Measurement setup (b) Arm measurement

TABLE I
The Extracted Optical Properties of Breast and Muscle Phantoms

Laser	Extracted Optical Properties (mm^{-1})							
	Breast Phantom				Muscle Phantom			
	HBS		LBS		HBS		LBS	
	μ_a	μ_s'	μ_a	μ_s'	μ_a	μ_s'	μ_a	μ_s'
681nm	0.00348	1.082	0.00346	1.125	0.02144	1.152	0.02478	1.082
783nm	0.00429	1.011	0.00454	1.026	0.02402	1.027	0.02196	0.94
806nm	0.0041	0.966	0.00466	0.949	0.02377	0.973	0.02214	0.891
823nm	0.00333	0.892	0.00377	0.911	0.02187	0.968	0.0244	0.895

with a well known two-distance, calibration independent method [5]. Another phantom, ISS1, was used to calibrate out the instrumental phase and amplitude contributions. Fig. 7(a) and Fig. 7(b) show the post-calibrated amplitude and phase values and their respective theoretically fitted results of the Breast and Muscle phantoms for all four lasers. As expected, the data from the Muscle phantom are noisier than those of the Breast phantom. This is because the Muscle phantom has a higher overall absorption efficient than the Breast phantom. Table I shows the extracted optical properties from the fitted diffusion theory of the Breast and Muscle phantoms including comparisons to those from the LBS. As can be seen, the maximum difference between the HBS and the LBS is 13.5%.

B. Recovered Concentration

We are able to utilize the extracted optical properties of tissues to recover physiological information. Although many near-infrared absorbing chromorphores do exist, the four main absorbers are oxyhemoglobin, deoxyhemoglobin, water, and lipid. Given their

TABLE II
Extracted Optical Properties of three India Ink phantoms by HBS and LBS

Laser	Extracted Optical Properties (mm^{-1})											
	0.05uL/mL				0.1uL/mL				0.175uL/mL			
	HBS		LBS		HBS		LBS		HBS		LBS	
	μ_a	μ_s'	μ_a	μ_s'	μ_a	μ_s'	μ_a	μ_s'	μ_a	μ_s'	μ_a	μ_s'
681nm	0.00682	0.875	0.00801	0.845	0.00868	1.099	0.01062	0.956	0.01687	1.132	0.01999	1.067
783nm	0.00675	0.719	0.00644	0.709	0.00881	0.921	0.00908	0.818	0.01725	0.964	0.01858	0.922
806nm	0.00694	0.682	0.00719	0.632	0.00893	0.872	0.00976	0.723	0.01764	0.873	0.01875	0.803
823nm	0.00739	0.653	0.00682	0.663	0.00894	0.818	0.00957	0.751	0.01748	0.835	0.01885	0.835

TABLE III
Recovered Concentration of India Ink from HBS and LBS

Phantom	Recovered Concentration of India Ink (uL/mL)	
	HBS	LBS
0.05uL/mL	0.07	0.07
0.10uL/mL	0.09	0.09
0.175uL/mL	0.17	0.18

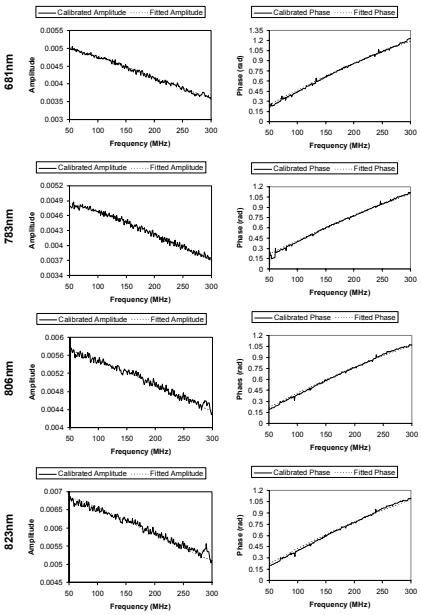

(a)

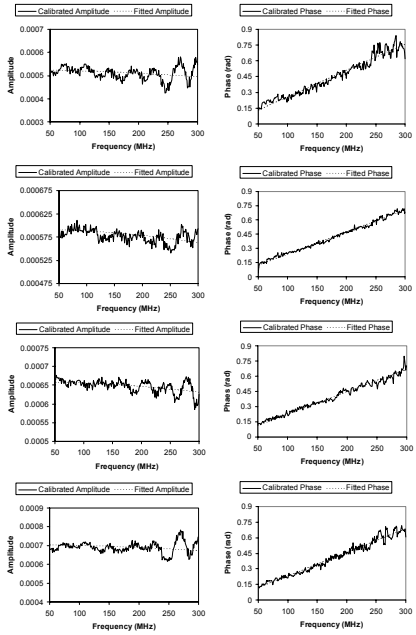

(b)

Fig. 7. Calibrated and Fitted Amplitude and Phase of (a) Breast (b) Muscle Phantoms

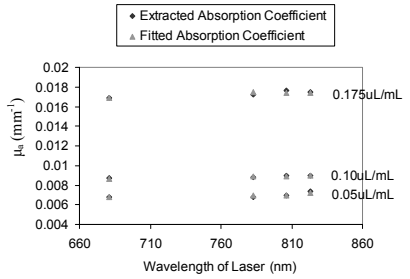

Fig. 8. Extracted and Fitted Absorption Coefficients of Three India Ink Phantom

distinct absorption spectra in the 650–1000nm band, we perform a linear least squares fitting to the recovered overall absorption to calculate the concentration of these absorbers. To validate the capabilities of our instrument, we performed studies on silicone phantoms with known volumes of Black India Ink. Black India Ink has a fairly flat broadband absorption spectrum between 650nm – 1000nm. Silicone has mainly two distinct absorption peaks, one minimal peak and one significant peak at approximately 720nm and 920nm, respectively. However, at the discrete wavelengths of these validation measurements, Black India Ink can be considered to be the only absorber while silicone absorption is negligible. We used Titanium Dioxide (TiO_2) as the scattering agent. A total of three 200mL silicone phantoms were made. The concentrations of Black India Ink used were 0.05μL/mL, 0.10μL/mL, and 0.175μL/mL. These three phantoms were measured with both the LBS and the HBS with the ISS1 phantom as the calibration reference. Table II shows the extracted optical properties of the three phantoms. Fig. 8 shows the extracted and fitted absorption coefficients of the 0.10L/mL phantom. The recovered concentrations of each India Ink phantom are shown in Table III. The results from the HBS are very comparable to the standard LBS. The recovered errors with both instruments is due to the very low volume (10, 20, and 35μL for 0.05μL/mL, 0.10μL/mL, and 0.175μL/mL phantoms, respectively) of India Ink used in these phantoms.

VI. Conclusions

This paper presents HBS, a miniature FDPM spectroscopy instrument with 681, 783, 806, and 823nm lasers. The full heterodyne structure increases device sensitivity and enables optical fiber coupling contact. This enables interfacing with the same measurement probe also used by the LBS, the reference instrument. Measurement results show HBS performs similar to the LBS. The improved user interface with Rappit and software architecture with Tapper facilitate the control of HBS and accelerates data collection. This instrument is not only ready for clinical trial but also serving as a platform on which a new generation of networked instruments can be built for real-time and imaging applications.

Acknowledgments: This work was supported in part by NIH under the NTROI Seed Grant and SBIR 34337, U54-CA105480 P41-RR01192, Henry T. Nicholas Fellowship, and NSF CAREER CNS-0448668.

References

[1] B. J. Tromberg, N. Shah, R. Lanning, A. Cerussi, J. Espinoza, T. Pham, L. Svaasand, and J. Butler, "Non-invasive *In Vivo* characterization of breast tumors using photon migration spectroscopy," *Neoplasia*, vol. 2, no. 1–2, pp. 26–40, Jan.–Apr. 2000.

[2] K.-S. No and P. H. Chou, "Mini-FDPM and Heterodyne Mini-FDPM: Handheld non-invasive breast cancer detectors based on frequency-domain photon migration," *IEEE Transactions on Circuits and Systems*, vol. 52, pp. 2672–2685, 2005.

[3] Q. Xie, J. Liu, and P. H. Chou, "Tapper: A lightweight scripting engine for highly constrained wireless sensor nodes," in *Proc. Information Processing in Sensor Networks*, April 2006, pp. 342–349.

[4] J. Hahn, Q. Xie, and P. H. Chou, "Rappit: A framework for the synthesis of host-assisted light-weight scripting engines for adaptive embedded systems," in *Proc. International Conference on Hardware Software Codesign and System Synthesis (Codes+ISSS)*, September 2005, pp. 315–320.

[5] T. H. Pham, O. Coquoz, J. B. Fishkin, E. Anderson, and B. Tromberg, "Broad bandwidth frequency domain instrument for quantitative tissue optical spectroscopy," *Review of Scientific Instruments*, vol. 71, no. 6, pp. 2500–2513, June 2000.